

# Current deformation and quantum inductance in mesoscopic capacitors

Y. Yin<sup>1,\*</sup>

<sup>1</sup>*Laboratory of Mesoscopic and Low Dimensional Physics,  
Department of Physics, Sichuan University, Chengdu, Sichuan, 610064, China  
(Dated: February 21, 2014)*

We present a theoretical analysis of finite frequency dynamics of a single-channel mesoscopic capacitor, which is composed by a quantum dot connected to an electron reservoir via a single quantum channel. At low frequencies, it is known that the Wigner-Smith delay time plays a dominant role and it can be interpreted as the time delay between current leaving the dot and the current entering the dot. At higher frequencies, we find that another characteristic time can also be important. It describes the deformation of the leaving current to the entering one and hence can be referred as the deformation time. By using a Hartree-Fock approximation to include the interactions in the dot, we compare the behavior of the deformation time to the Wigner-Smith delay time as function of the Fermi energy. While both of them show distinct oscillations, the most striking difference is that the Wigner-Smith delay time is positive defined, while the deformation time can be positive, negative and zero. We further show that the deformation time can have a pronounced impact on the quantum inductance of the mesoscopic capacitor, leading to negative quantum inductance at nonzero temperatures.

PACS numbers: 73.23.-b, 72.10.-d, 72.21.La

## I. INTRODUCTION

The understanding of the low-frequency ac conductance of quantum conductors has attracted renewed interest in recent years.<sup>1-5</sup> In the linear response regime, it has been demonstrated that the ac conductance is directly related to the Wigner-Smith delay time of electrons.<sup>1</sup> This offers a means to investigate the charge relaxation process on a mesoscopic scale.<sup>6</sup> In the non-linear regime, the control and manipulation of a single electron have been realized at gigahertz frequencies.<sup>3-5</sup> This opens the way to the new generation devices which can serve as building blocks for quantum electron optics and quantum information processing.<sup>7-9</sup>

As an elementary structure in this area, the mesoscopic capacitor<sup>10,11</sup> plays a central role. It is composed by a quantum dot (QD) and an electron reservoir, connected via a quantum point contact (QPC) as illustrated in Fig. 1. The QD is capacitively coupled to a metallic electrode, which forms a geometrical capacitor with capacitance  $C_e$ . As the dc response is completely suppressed in the mesoscopic capacitor, such system is quite suitable to study the ac response.<sup>12</sup> The low-frequency ac conductance of the mesoscopic capacitor has been extensively studied both theoretically<sup>13-21</sup> and experimentally.<sup>1</sup> It has been found that the Wigner-Smith delay time  $\tau_W$  is crucial to the ac conductance up to the second order of the frequency  $\omega$ , leading to a quantum capacitance  $C_q = \frac{e^2}{h} \tau_W$  and a universal charge relaxation resistance  $R_q = \frac{h}{2e^2}$  for the single-channel mesoscopic capacitor. The corresponding ac conductance  $G(\omega)$  can be expressed as

$$G(\omega) = -i\omega C_\mu(1 + i\omega R_q C_\mu) + O(\omega^2), \quad (1)$$

where  $C_\mu = 1/(1/C_e + 1/C_q)$  is usually referred as the electrochemical capacitance.<sup>10</sup>

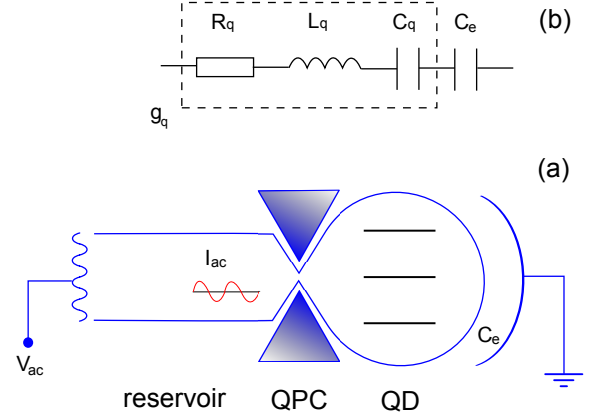


FIG. 1. (Color online) (a) Mesoscopic capacitor. The tunneling between the QD and the reservoir are controlled via the QPC. An external ac field  $V_{ac}$  causes the carrier exchange between the QD and the reservoir, leading to an ac current  $I_{ac}$ . The QD and the metallic electrode on the right are capacitively coupled, which does not permit carrier exchange. (b) The low-frequency equivalent circuit of the mesoscopic capacitor. The geometrical capacitance  $C_e$  (formed between the QD and the right electrode) is in series with the quantum conductance  $g_q$ . Up to the third order of the frequency,  $g_q$  can be characterized by a quantum capacitor  $C_q$ , a charge relaxation resistance  $R_q$  and a quantum inductance  $L_q$ .

The above result highlights the importance of the Wigner-Smith delay time on the charge relaxation process of the mesoscopic capacitor at low frequencies. Such effect can be vividly interpreted within the delayed current picture introduced by Ringel *et al.*<sup>16</sup> They show that the total current of the mesoscopic capacitor can be interpreted in terms of an incoming current and an outgoing current. While the incoming current responds instantaneously to the external driving field, the outgo-

ing current is delayed by  $\tau_W$  with respect to the incoming one. Such picture well captures the behavior of ac conductance up to the second order of the frequency. It is worth noting that at higher frequencies, the effect of the Wigner-Smith delay time are expected to be more pronounced. Wang *et al.* have shown that up to the third order of the frequency, it can lead to a quantum inductance  $L_q = R_q\tau_W/12$  under the resonance condition when the QD levels are aligned with the Fermi energy of the reservoir. The corresponding  $G(\omega)$  can be written as<sup>22</sup>

$$G(\omega) = -i\omega C_\mu(1 + i\omega R_q C_\mu - \omega^2 C_\mu^2 R_q^2 + \omega^2 C_\mu L_q) + O(\omega^3). \quad (2)$$

However, since not all the transport processes can be well captured through the Wigner-Smith delay time, especially on the short-time scales,<sup>23–26</sup> it is natural to ask: is there any other characteristic time that can play a role on the ac conductance at higher frequencies? This question is the main motivation of this work. To study this question, we reexamine the delayed current picture and find that such current delay can only describe the behavior of the ac conductance  $G(\omega)$  up to the second order of the frequency. As the frequency goes higher, another effect—the current deformation—can be important and a new characteristic time—the deformation time  $\tau_S$ —is introduced to evaluate the magnitude of such deformation. As a consequence,  $\tau_S$  can manifest itself in the quantum inductance  $L_q$  as

$$L_q = R_q\tau_W[2(\frac{\tau_S}{\tau_W})^3 + \frac{1}{6}]. \quad (3)$$

The  $L_q$  obtained by Wang *et al.* can be treated as a specific case of Eq. (3) under the resonance condition. To have a better understanding of the deformation effect and its impact on the quantum inductance  $L_q$ , we further compare the behavior of the Wigner-Smith delay time  $\tau_W$  and the deformation time  $\tau_S$  within the Hartree-Fock approximation to include the interactions in the dot. We find that although both  $\tau_W$  and  $\tau_S$  can exhibit oscillations as function of the Fermi energy, the most striking difference between them is that  $\tau_W$  is always positive-defined, while  $\tau_S$  can be positive, negative and zero. Specifically,  $\tau_S$  can reach large negative values at nonzero temperatures. Due to the impact of the negative  $\tau_S$ , a sign-changing of the quantum inductance  $L_q$  can be obtained at nonzero temperatures. These results indicate the importance of the deformation time  $\tau_S$  on the ac conductance of the mesoscopic capacitor at higher frequencies.

The paper is organized as follows: In Sec. II, we generalize the delayed current picture to include the current deformation effect. In Sec. III, we present the Hamiltonian used in the numerical calculation, which has been successfully used in the study of the quantum capacitance of the mesoscopic capacitor. The numerical results are discussed in Sec. IV. We summarized in Sec. V.

## II. DELAYE-DEFORMED CURRENT

In this section, we generalize the delayed current picture to include the effect of current deformation and discuss its relation to the quantum inductance  $L_q$  of the mesoscopic capacitor.

Following the scattering-formalism approach,<sup>27</sup> the current operator for the single-channel mesoscopic capacitor can be decomposed into an incoming part  $\hat{I}_+$  and outgoing part  $\hat{I}_-$ , which can be expressed as

$$\hat{I}(t) = \hat{I}_+(t) - \hat{I}_-(t), \quad (4)$$

$$\hat{I}_+(t) = \frac{e}{2\pi\hbar} \int dE \hat{n}_+(E, t), \quad (5)$$

$$\hat{I}_-(t) = \frac{e}{2\pi\hbar} \int dE \hat{n}_-(E, t), \quad (6)$$

where  $\hat{n}_+(\hat{n}_-)$  is the operator describing the occupation numbers of the incoming(outgoing) channel. They can be written as

$$\hat{n}_+(E, t) = \int d\omega e^{-i\omega t} \hat{a}^\dagger(E - \hbar\omega/2) \hat{a}(E + \hbar\omega/2), \quad (7)$$

$$\hat{n}_-(E, t) = \int d\omega e^{-i\omega t} \hat{b}^\dagger(E - \hbar\omega/2) \hat{b}(E + \hbar\omega/2), \quad (8)$$

where  $\hat{a}(E)[\hat{b}(E)]$  and  $\hat{a}^\dagger(E)[\hat{b}^\dagger(E)]$  are the creation and annihilation operators of electrons in the incoming(outgoing) channel with energy  $E$ , respectively.

For the case of elastic scattering, the operators  $\hat{a}$  and  $\hat{b}$  are related via the scattering matrix, which can be described by just a pure phase factor  $\phi$  for the single-channel system,<sup>28–30</sup>

$$\hat{b}(E) = S(E)\hat{a}(E), \quad (9)$$

$$S(E) = e^{i\phi(E)}. \quad (10)$$

By substituting Eqs. (9) and (10) into Eqs. (7) and (8), one obtains the relation between the occupation number operator of incoming and outgoing electrons,

$$\hat{n}_-(E, t) = \int dt' \hat{n}_+(E, t') A(E, t - t'), \quad (11)$$

where the effects of the scattering are attributed to the integral kernel  $A(E, t)$ . It can be expressed in terms of the scattering phase factor as

$$A(E, t) = \int \frac{d\omega}{2\pi} e^{-i\omega t} e^{-i[\phi(E - \hbar\omega/2) - \phi(E + \hbar\omega/2)]}. \quad (12)$$

If the scattering phase factor  $\phi(E)$  is slow-varying with respect to the energy  $E$ , the integral kernel  $A(E, t)$  can be expanded with respect to the frequency  $\omega$ , yielding the low frequency expansion

$$A(E, t) = \int \frac{d\omega}{2\pi} e^{-i\omega t} e^{i\omega\tau_W + i\omega^3\tau_S^3 + O(\omega^3)}. \quad (13)$$

The two parameters  $\tau_W$  and  $\tau_S$  in Eq. (13) can be written as

$$\tau_W = \hbar \phi'(E), \quad (14)$$

$$\tau_S = \frac{\hbar}{2} \sqrt[3]{\frac{\phi'''(E)}{3}}, \quad (15)$$

where  $\phi'(E)$  and  $\phi'''(E)$  represent the first-order and third-order derivatives of the phase factor with respect to the energy  $E$ , respectively. Note that  $\tau_W$  is just the Wigner-Smith delay time, while the other parameter  $\tau_S$  also has dimension of time. From Eqs. (11-15), one can see that at low frequencies, the effects of the scattering can be described by two characteristic times  $\tau_W$  and  $\tau_S$ .

At sufficient low frequencies when the  $\tau_S$ -term in the exponent in Eq. (13) can be ignored, Eqs. (11) and (13) indicate that the effect of the scattering merely introduce a time delay  $\tau_W$  between the incoming and outgoing currents, while the two currents have the same profile. This interpretation agrees with the delayed current picture introduced by Ringel *et al.*<sup>16</sup> However, at higher frequencies when the  $\tau_S$ -term becomes important, the scattering makes the outgoing current not only delayed, but also deformed from the incoming one. The magnitude of the deformation is quantitatively described by the parameter  $\tau_S$ , which has dimension of time. Hence  $\tau_S$  can be regarded as the "deformation" time. From the above discussion, one can see that the delayed current picture can become inadequate at higher frequencies and one has to take the deformation effect into consideration. The corresponding quantum conductance including the deformation effect can be calculated as<sup>16</sup>

$$g_q(\omega) = \frac{1}{\hbar\omega} \int_0^\infty dt e^{i(\omega+i\eta)t} \langle [\hat{I}(t), \hat{I}(0)] \rangle, \quad (16)$$

where  $\eta \rightarrow 0^+$  and  $\langle \dots \rangle$  represents the thermal average over the Fermi distribution. Substituting Eqs. (4-15) in Eq. (16), one has

$$g_q(\omega) = \frac{e^2}{h} (1 - e^{i\omega\tau_W} e^{i\omega^3\tau_S^3}), \quad (17)$$

where both the current delay and deformation has been taken into consideration.

Now let us turn to discuss the impact of the current deformation on the low-frequency ac conductance of the mesoscopic capacitor, which is usually described by equivalent RLC circuits.<sup>22</sup> This can be done by matching the impedance of the mesoscopic capacitor<sup>1,10</sup>

$$Z(\omega) = \frac{1}{g_q(\omega)} - \frac{1}{i\omega C_e}, \quad (18)$$

to the corresponding formula for a classical RLC circuits

$$Z(\omega) = \frac{i}{\omega} \left( \frac{C_q C_e}{C_q + C_e} - i\omega R_q - \omega^2 L_q \right), \quad (19)$$

where  $g_q$  is given by Eq. (17). By comparing Eq. (18) to Eq. (19), one obtains the quantum capacitor  $C_q$ , charge

relaxation resistance  $R_q$  and the quantum inductance  $L_q$  as

$$C_q = \frac{e^2}{h} \tau_W, \quad (20)$$

$$R_q = \frac{h}{2e^2}, \quad (21)$$

$$L_q = R_q \tau_W \left[ 2 \left( \frac{\tau_S}{\tau_W} \right)^3 + \frac{1}{6} \right]. \quad (22)$$

Note that the quantum capacitance  $C_q$  is solely determined by the Wigner-Smith delay time  $\tau_W$ , while the quantum inductance  $L_q$  is not only related to  $\tau_W$ , but also depends on the deformation time  $\tau_S$ .

From the above discussion, one can see that up to the third order of the frequency, the ac conductance of the mesoscopic capacitor can be interpreted in terms of two effects: the current delay and current deformation. At low frequencies, the current deformation plays a minor role and hence is irrelevant to the quantum capacitance and charge relaxation resistance. At higher frequencies, the current deformation can be important, which manifests itself in the quantum inductance of the mesoscopic capacitor.

Most previous works have focused on the quantum capacitance  $C_q$ ,  $R_q$  and  $\tau_W$ , while the quantum inductance  $L_q$  and  $\tau_S$  are much less studied. In the next section, we will present a numerical model to study the behavior of  $L_q$  and  $\tau_S$  within the Hartree-Fock approximation to include the interactions in the QD.

### III. HAMILTONIAN

The Hamiltonian of the mesoscopic capacitor illustrated in Fig. 1 can be written as<sup>16</sup>

$$H = H_L + H_D + H_{LD}, \quad (23)$$

where  $H_L$ ,  $H_D$  and  $H_{LD}$  describe the reservoir, the QD and their coupling, respectively. The reservoir Hamiltonian  $H_L$  is derived from a one-dimensional tight-binding model, which can be written as

$$H_L = \int dk \varepsilon(k) a_k^\dagger a_k, \quad (24)$$

where  $\varepsilon(k) = -2t_0 \cos(k)$  is the dispersive relation with  $t_0$  being the hopping between adjacent sites in the lead. The Hamiltonian of the QD, including the single-particle part and interactions, can be expressed as

$$H_D = \sum_{n=1}^{n_d} \epsilon_n d_n^\dagger d_n + \frac{E_C}{2} (\hat{N} - \frac{n_d}{2})^2, \quad (25)$$

where  $\epsilon_n = n\Delta$  with  $\Delta$  being the level spacing.  $E_C = e^2/C_e$  describes the charging energy with  $C_e$  being the geometrical capacitance.  $\hat{N} = \sum_{n=1}^{n_d} d_n^\dagger d_n$  is the number operator of the electrons in the QD with  $n_d$  denoting the

number of QD levels. The coupling  $H_{LD}$  can be written as

$$H_{LD} = \sum_n \int dk (t_{kn} d_n^\dagger a_k + \text{H.c.}), \quad (26)$$

with  $t_{kn}$  being the coupling matrix element.

The quantum admittance  $g_q(\omega)$  can be calculated in the wide-band-limit<sup>31–33</sup> as

$$g_q(\omega) = -i \frac{e^2}{h} \int d\omega' \text{Tr}[G_D^r(\omega + \omega') \frac{\Gamma}{h} G_D^a(\omega')] \times [f(\omega') - f(\omega + \omega')], \quad (27)$$

where  $G_D^{r/a}(\omega)$  represents the equilibrium retarded/advanced Green function of the QD while  $\Gamma$  describes the level-width function of the QD due to the coupling to the lead.<sup>31</sup>  $f(\omega) = 1/[1 + \exp(\beta(\hbar\omega - E_F))]$  represents the equilibrium electron distribution, with  $E_F$  being the Fermi level and  $\beta = 1/(k_B T)$  being the inverse temperature.  $k_B$  is the Boltzmann constant and  $T$  is the temperature. The Taylor expansion of  $g_q(\omega)$  with respect to the frequency reads

$$g_q(\omega) = e_0 + e_1\omega + e_2\omega^2 + O(\omega^3), \quad (28)$$

$$e_0 = - \int d\omega' f'(\omega) \text{Tr}[G_D^r(\omega) \frac{\Gamma}{h} G_D^a(\omega)], \quad (29)$$

$$e_1 = - \int d\omega' \frac{f'(\omega)}{2} \text{Tr}[(G_D^r(\omega))' \frac{\Gamma}{h} G_D^a(\omega) - G_D^r(\omega) \frac{\Gamma}{h} (G_D^a(\omega))'], \quad (30)$$

$$e_2 = - \int d\omega' \frac{f'(\omega)}{6} \text{Tr}[(G_D^r(\omega))'' \frac{\Gamma}{h} G_D^a(\omega) + G_D^r(\omega) \frac{\Gamma}{h} (G_D^a(\omega))'' - (G_D^r(\omega))' \frac{\Gamma}{h} (G_D^a(\omega))'], \quad (31)$$

where  $(G_D^{r/a}(\omega))'$  and  $(G_D^{r/a}(\omega))''$  represent the first-order and second-order derivatives of the retarded/advanced QD Green function with respect to the frequency  $\omega$ .

By substituting Eqs. (28-31) into Eq. (18) and comparing to Eq. (19-22), one obtains the quantum capacitor  $C_q$ , charge relaxation resistance  $R_q$  and the quantum inductance  $L_q$  as

$$C_q = \frac{e^2}{h} e_0, \quad (32)$$

$$R_q = \frac{\tau_W}{2C_q}, \quad (33)$$

$$L_q = R_q \tau_W [2(\frac{\tau_S}{\tau_W})^3 + \frac{1}{6}], \quad (34)$$

where the two characteristic time  $\tau_W$  and  $\tau_S$  can be expressed as

$$\tau_W = -2i \frac{e_1}{e_0}, \quad (35)$$

$$\tau_S = \sqrt[3]{\frac{5}{12} - \frac{e_0 e_2}{2e_1^2}}. \quad (36)$$

To obtain  $C_q$ ,  $R_q$  and  $L_q$ , one needs to find the equilibrium retarded/advanced QD Green function  $G_D^{r/a}$ . They can be calculated self-consistently within the Hartree-Fock approximation as<sup>13,16</sup>

$$G_D^r = [\hbar\omega - H + \frac{i\gamma}{2h}]^{-1}, \quad (37)$$

$$H_{mn} = \delta_{mn}d + \frac{EC}{h} (\delta_{nm} \sum_{\bar{n}} Q_{\bar{n}\bar{n}} - Q_{nm}), \quad (38)$$

$$Q_{mn} = - \int \frac{d\omega}{\pi} f(\omega) \text{Im}[G_D^r]_{mn}. \quad (39)$$

In the calculation, we have assume all the QD levels couples to the lead with the same strength, i.e.,  $\Gamma_{mn} = \gamma$ .<sup>12,16</sup> Following Refs. 12 and 34, we choose the coupling  $\gamma$  as

$$\gamma = \frac{\Delta}{\pi D} (2 - D - 2\sqrt{1 - D}), \quad (40)$$

where  $D$  describes the probability for transmission through the QPC. It can be related to the Fermi energy  $E_F$  in the lead as<sup>35</sup>

$$D = \frac{1}{1 + e^{-aE_F/\Delta}}, \quad (41)$$

with  $a$  being a constant depends on the detail structure of the QPC potential.

It is worth mentioning that the we can reproduce the result of Wang *et al.* in Ref. 22 by applying the above equations to a simplified single-level QD model. For the QD with one level  $E_0$ , the retarded/advanced QD Green function can be written as  $G_D^{r/a}(\omega) = 1/(\hbar\omega - E_0 \pm \gamma/2)$ . With this Green function, Eqs. (28-36) give

$$C_q = \frac{e^2}{h} \tau_W, \quad (42)$$

$$R_q = \frac{h}{2e^2}, \quad (43)$$

$$L_q = \frac{R_q \tau_W}{12}, \quad (44)$$

where

$$\tau_W = \frac{4}{\gamma}, \quad (45)$$

$$\tau_S = -\frac{2}{\sqrt[3]{3}} \frac{1}{\gamma}. \quad (46)$$

In the above calculation, we have set the temperature  $T = 0K$  and the Fermi level is chosen to be at resonance with the QD:  $E_F = E_0$ . Eq. (44) agrees with the result in Ref. 22.

For QD with multi-levels and interactions, the behavior of the quantum inductance  $L_q$  and the deformation time  $\tau_S$  will be more complicated. These are studied in details in the next section.

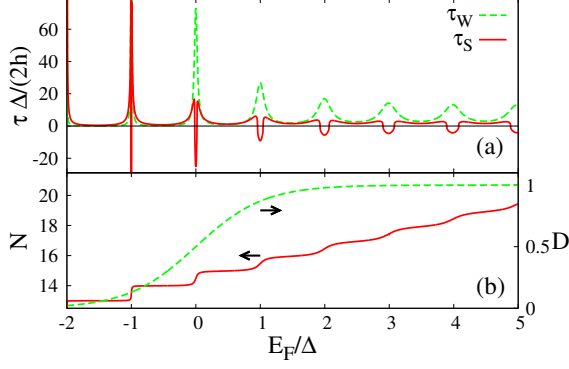


FIG. 2. (Color online) (a) The deformation time  $\tau_S$  (red solid curve) and the Wigner-Smith delay time  $\tau_W$  (green dashed curve) as function of the Fermi energy  $E_F$  at zero temperature. The black line indicates the zero value. (b) The corresponding total dot charge  $N$  of the QD (red solid curve) and the transmission probability  $D$  through the QPC (green dashed curve) as function of the Fermi energy at zero temperature. The charging energy  $E_C$  is set to 0 for both figures.

#### IV. NUMERICAL RESULTS

The computations in this section are performed for the QD with 29 levels. The parameter  $a$  of the QPC is chosen to be 1.9. The Fermi energy  $E_F$  and the QD charging energy  $E_C$  are all measured in units of the QD level spacing  $\Delta$  and the inverse temperature  $\beta = 1/(k_B T)$  is measured in units of  $1/\Delta$ .

Let us first concentrate on the dependence of  $\tau_W$  and  $\tau_S$  on the Fermi energy  $E_F$  without the charging energy  $E_C$ . In Fig. 2, we show the zero-temperature  $\tau_W$  and  $\tau_S$  as function of the Fermi energy  $E_F$  with the charging energy  $E_C = 0$  [Fig. 2(a)]. The corresponding total dot charge  $N$  and the probability for transmission through the QPC  $D$  are also plotted for comparison [Fig. 2(b)]. From the figure, one can see that both  $\tau_W$  and  $\tau_S$  exhibits distinct oscillations as  $E_F$  varies. However, the detail structure of these oscillations are different. When the QPC is close to pinch-off ( $D \ll 1$ ),  $\tau_W$  exhibits a sharp single peak at the resonance where the transfer of an electron into the QD is permitted. As the QPC is opened ( $D \rightarrow 1$ ), the peak is broadened and its height is decreased. Such behavior has been observed in the experiment via the capacitance oscillations.<sup>1</sup> On the contrary,  $\tau_S$  exhibits a sharp dip at the resonance when  $D \ll 1$ , with two peaks appearing at both sides of the dip. As the QPC is opened, such dip-double-peak structure is strongly suppressed into smooth shallow valleys.

The most striking difference between  $\tau_W$  and  $\tau_S$  from Fig. 2 is that  $\tau_W$  is positive-defined, while  $\tau_S$  is not. By comparing  $\tau_S$  to the zero value indicated by the black line, one can see that  $\tau_S$  is only positive far from the resonance, while it becomes negative at the vicinity of the resonance where  $\tau_S$  exhibits dips(valleys). Hence a sign-

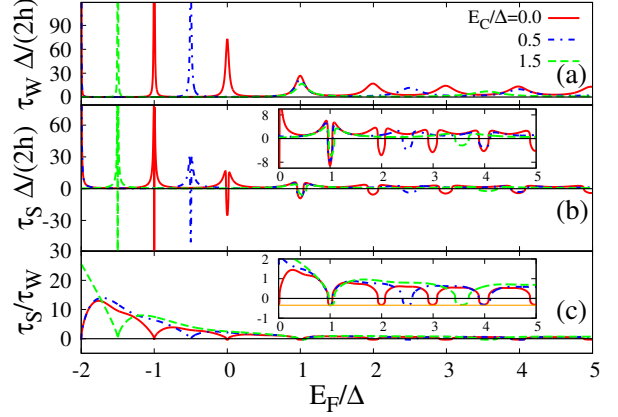


FIG. 3. (Color online) The zero-temperature  $\tau_W$  (a),  $\tau_S$  (b) and their ratio  $\tau_S/\tau_W$  (c) as function of the Fermi energy  $E_F$ . Curves with different colors and line types correspond to different charging energy  $E_C$ . The zoom of  $\tau_S(\tau_S/\tau_W)$  in the region  $E_F/\Delta \in [0, 5]$  is plotted in the inset of (b) [inset of (c)]. The orange solid line in the inset of (c) indicates the constant value  $-1/(2\sqrt[3]{3})$  obtained from the simplified single-level QD model. In all figures, the black solid line indicates the zero value.

changing for  $\tau_S$  can occurs as  $E_F$  varies around the resonance. Specifically,  $\tau_S$  can become zero at some points, corresponding to the case when the current deformation can be ignored at low frequencies.

It is known that by increasing the charging energy  $E_C$ , the oscillation of  $\tau_W$  can be smeared out.<sup>16,36</sup> Similar effect also occurs for  $\tau_S$ . To show this, we plot the zero-temperature  $\tau_W$  and  $\tau_S$  as function of  $E_F$  for different  $E_C$  in Fig. 3. From Fig. 3(a), one can see that as the charging energy  $E_C$  increasing, the peaks in  $\tau_W$  are broadened and their height is decreased, leading to a suppression of the oscillation of  $\tau_W$ . Similar suppression can also be found for  $\tau_S$ , which can be seen in Fig. 3(b). From the figure, one can see that the dips(valleys) at the vicinity of the resonances in  $\tau_S$  become more shallow and wider as  $E_C$  increasing, while the two side peaks around the resonance are also smeared out [This can be better seen in the inset of Fig. 3(b)]. This result indicates a suppression of the oscillation of  $\tau_S$  also occurs as  $E_C$  increasing.

Due to the suppression of the oscillations,  $\tau_S$  at the vicinity of the resonance becomes less negative for large  $E_C$ . Thus one may wonder if  $\tau_S$  can become positive at the resonance for large  $E_C$  and the sign-changing of  $\tau_S$  around the resonance can also vanish as  $E_C$  increasing. To answer this question, we plot the ratio  $\tau_S/\tau_W$  as function of  $E_F$  for different  $E_C$  in Fig. 3(c). From the figure, one can see that although both the oscillations of  $\tau_S$  and  $\tau_W$  tend to vanish as  $E_C$  increasing, the ratio  $\tau_S/\tau_W$  always exhibit distinct oscillations despite the increasing of  $E_C$ .  $\tau_S/\tau_W$  is always positive far from the resonance and negative at the vicinity of the resonance. The magnitude of the oscillations is even slightly increasing as

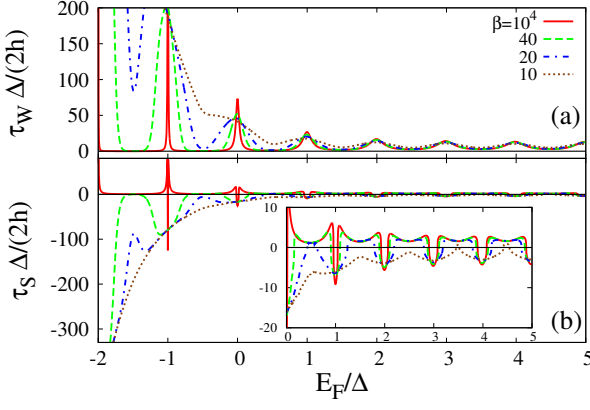


FIG. 4. (Color online) (a) The Wigner-Smith delay time  $\tau_W$  as function of the Fermi energy  $E_F$  for different inverse temperature  $\beta$ . (b) The deformation time  $\tau_S$  as function of the Fermi energy  $E_F$  for different inverse temperature  $\beta$ . Curves with different colors and line types correspond to different inverse temperature  $\beta$ . The zoom of  $\tau_S$  in the region  $E_F/\Delta \in [0, 5]$  is plotted in the inset of (b). In all figures, the black solid line indicates the zero value.

$E_C$  increasing. These can be seen more clearly by comparing the curves corresponding to different  $E_C$  in the inset of Fig. 3(c). As  $\tau_W$  is positive-defined, this result indicates that the sign-changing of  $\tau_S$  preserves and  $\tau_S$  is negative-defined at the vicinity of the resonance even for large charging energy  $E_C$ .

It is worth noting that from Fig. 3(c), one can also see that the ratio  $\tau_S/\tau_W$  at the resonance is almost unchanged as  $E_C$  varies. It is always close and slightly above the constant value  $-1/(2\sqrt[3]{3})$  [indicated by the orange solid line in the inset of Fig. 3(c)], which agrees with the ratio from the simplified single-level QD model described in Sec. III [Eqs. (45) and (46)]. According to Eq. (34), this means that the quantum inductance  $L_q$  has the lower bound  $R_q\tau_W/12$  at zero temperature and hence it is positive-defined.

Then it is natural to ask if it is possible to have a negative quantum inductance in the mesoscopic capacitor. We find that although this is difficult to be achieved at zero temperature, it is easy to have negative quantum inductance at nonzero temperatures. Before we discuss this, let us first show the behavior of  $\tau_W$  and  $\tau_S$  at nonzero temperatures. In Fig. 4,  $\tau_W$  [Fig. 4(a)] and  $\tau_S$  [Fig. 4(b)] as function of the Fermi energy  $E_F$  for different inverse temperature  $\beta$  are plotted with different curves. The charging energy  $E_C$  is set to 0. From the figure, one can see that the oscillations of both  $\tau_W$  and  $\tau_S$  are smeared out as the inverse temperature  $\beta$  decreasing. However, they have different tendency. The overall  $\tau_W$  tends to increase as  $\beta$  decreasing, while the corresponding  $\tau_S$  tends to decrease to large negative values. Note that for a given inverse temperature  $\beta$ , it is more easy to have negative  $\tau_S$  when the QPC is close to pinch-off

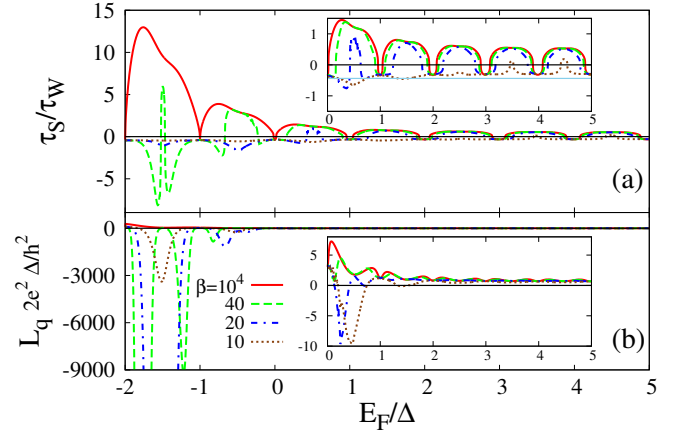


FIG. 5. (Color online) (a) The ratio  $\tau_S/\tau_W$  as function of the Fermi energy  $E_F$  for different inverse temperature  $\beta$ . (b) The corresponding quantum inductance  $L_q$  as function of the Fermi energy  $E_F$  for different inverse temperature  $\beta$ . Curves with different colors and line types correspond to different inverse temperature  $\beta$ . The zoom of  $\tau_S/\tau_W(L_q)$  in the region  $E_F/\Delta \in [0, 5]$  is plotted in the inset of (a) [inset of (b)]. The skyblue solid line in the inset of (a) indicates the constant value  $-1/(\sqrt[3]{12})$ . In all figures, the black solid line indicates the zero value and the charging energy  $E_C$  is set to 0.

( $D \ll 1$ ).

Now let us turn to discuss the quantum inductance. According to Eq. (34), the negative inductance corresponds to the condition  $\tau_S/\tau_W < -1/\sqrt[3]{12}$ . In Fig. 5, we plot the ratio  $\tau_S/\tau_W$  [Fig. 5(a)] and the corresponding quantum inductance  $L_q$  [Fig. 5(b)] as function of  $E_F$  for different inverse temperatures  $\beta$  with different curves. From Fig. 5(a), one can see that for small enough  $\beta$ ,  $\tau_S/\tau_W$  can go below the value  $-1/\sqrt[3]{12}$  [indicated by the skyblue line in the inset of Fig. 5(a)] in some regions, which can be better seen from the inset of Fig. 5(a). This leads to the negative quantum inductance  $L_q$  in the corresponding regions, which can be seen by comparing Fig. 5(b) to Fig. 5(a). Note that it is more easy to have negative quantum inductance  $L_q$  when the QPC is close to pinch-off ( $D \ll 1$ ).

Thus at nonzero temperatures, it is possible to observe a sign-changing of  $L_q$  as the QPC is closed, which is due to the contribution of the deformation time  $\tau_S$ . The sign-changing of  $L_q$  can even be enhanced by the increasing of the charging energy  $E_C$ , which can be seen in Fig. 6. In the figures, we plot the ratio  $\tau_S/\tau_W$  and the corresponding quantum inductance  $L_q$  with charging energy  $E_C/\Delta = 0.5$ , while other parameters are the same as for Fig. 5. By comparing Fig. 6 to Fig. 5, one can see that in some regions, larger  $E_C$  can lead to more negative quantum inductance  $L_q$ .



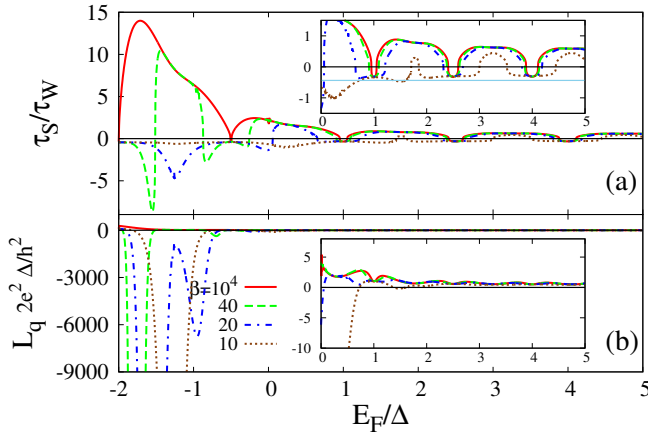


FIG. 6. (Color online) (a) The ratio  $\tau_S/\tau_W$  as function of the Fermi energy  $E_F$  for different inverse temperature  $\beta$ . (b) The corresponding quantum inductance  $L_q$  as function of the Fermi energy  $E_F$  for different inverse temperature  $\beta$ . Curves with different colors and line types correspond to different inverse temperature  $\beta$ . The zoom of  $\tau_S/\tau_W(L_q)$  in the region  $E_F/\Delta \in [0, 5]$  is plotted in the inset of (a) [inset of (b)]. The skyblue solid line in the inset of (a) indicates the constant value  $-1/(\sqrt[3]{12})$ . In all figures, the black solid line indicates the zero value and the charging energy  $E_C$  is set to 0.5.

## V. SUMMARY

In this work, we have examined the characteristic times which describe the finite frequency dynamics of the mesoscopic capacitors. By generalizing the delayed current

picture introduced by Ringel *et al.*, we found that the Wigner-Smith delay time can only capture the ac response of the mesoscopic capacitor up to the second order of the frequency. At higher frequencies, a new time scale—the deformation time—has to be taken into consideration. The deformation time indicates that due to the scattering, the profile of the outgoing current from the dot is distorted from the incoming one. To have a better understanding of the deformation time, we performed further numerical studies within the Hartree-Fock approximation to include the interactions in the QD. The deformation time was found to have different behaviors from the Wigner-Smith delay time. The most striking difference is that it can change the sign around the resonances, while the Wigner-Smith delay time is positive-defined. Although the deformation time is irrelevant up to the second order of the frequency, it can affect the ac response of the mesoscopic capacitor at high frequencies. Specifically, we found that it can manifest itself in the quantum inductance of the mesoscopic capacitor. Due to the impact of the deformation time on the quantum inductance, it is possible to have negative quantum inductance at nonzero temperatures. These results highlight the importance of the deformation time on the ac response of the mesoscopic capacitors.

## ACKNOWLEDGMENTS

This work was supported by Key Program of National Natural Science Foundation of China under Grant No. 11234009 and National Key Technology R&D Program of China under Grant No. 20-1125ZCKF.

\* Author to whom correspondence should be addressed; yin80@scu.edu.cn.

<sup>1</sup> J. Gabelli, J.-M. Berroir, G. Fève, B. Plaças, Y. Jin, B. Etienne, and D. C. Glattli, *Science* **313**, 499 (2006).

<sup>2</sup> J. Gabelli, G. Fève, T. Kontos, J.-M. Berroir, B. Plaças, D. C. Glattli, B. Etienne, Y. Jin, and M. Büttiker, *Phys. Rev. Lett.* **98**, 166806 (2007).

<sup>3</sup> G. Fève, A. Mahè, J.-M. Berroir, T. Kontos, B. Plaças, D. C. Glattli, A. Cavanna, B. Etienne, and Y. Jin, *Science* **316**, 5828 (2007).

<sup>4</sup> E. Bocquillon, V. Freulon, J.-M. Berroir, P. Degiovanni, B. Plaças, A. Cavanna, Y. Jin, and G. Fève, *Science* **339**, 1054 (2013).

<sup>5</sup> J. Dubois, T. Jullien, P. Rouleau, F. Portier, P. Roche, A. Cavanna, Y. Jin, W. Wegscheider, and D. C. Glattli, *Nature* **502**, 659 (2013).

<sup>6</sup> J. Gabelli, G. Fève, J.-M. Berroir, and B. Plaças, *Rep. Prog. Phys.* **75**, 126504 (2012).

<sup>7</sup> A. Mahè, F. D. Parmentier, E. Bocquillon, J.-M. Berroir, D. C. Glattli, T. Kontos, B. Plaças, G. Fève, A. Cavanna, and Y. Jin, *Phys. Rev. B* **82**, 201309 (2010).

<sup>8</sup> F. D. Parmentier, E. Bocquillon, J.-M. Berroir, D. C. Glattli, B. Plaças, G. Fève, M. Albert, C. Flindt, and M. Büttiker, *Phys. Rev. B* **85**, 165438 (2012).

<sup>9</sup> E. Bocquillon, F. D. Parmentier, C. Grenier, J.-M. Berroir, P. Degiovanni, D. C. Glattli, B. Plaças, A. Cavanna, Y. Jin, and G. Fève, *Phys. Rev. Lett.* **108**, 196803 (2012).

<sup>10</sup> M. Büttiker, H. Thomas, and A. Prêtre, *Phys. Lett. A* **180**, 364 (1993).

<sup>11</sup> M. Büttiker, *J. Phys.: Condens. Matter* **5**, 9361 (1993).

<sup>12</sup> M. Büttiker and S. E. Nigg, *Nanotechnology* **18**, 044029 (2007).

<sup>13</sup> S. E. Nigg, R. López, and M. Büttiker, *Phys. Rev. Lett.* **97**, 206804 (2006).

<sup>14</sup> S. E. Nigg and M. Büttiker, *Phys. Rev. B* **77**, 085312 (2008).

<sup>15</sup> M. Moskalets, P. Samuelsson, and M. Büttiker, *Phys. Rev. Lett.* **100**, 086601 (2008).

<sup>16</sup> Z. Ringel, Y. Imry, and O. Entin-Wohlman, *Phys. Rev. B* **78**, 165304 (2008).

<sup>17</sup> S. E. Nigg and M. Büttiker, *Phys. Rev. Lett.* **102**, 236801 (2009).

<sup>18</sup> C. More and K. Le Hur, *Nat. Phys.* **6**, 697 (2010).

<sup>19</sup> Y. Hamamoto, T. Jonckheere, T. Kato, and T. Martin, *Phys. Rev. B* **81**, 153305 (2010).

<sup>20</sup> M. Lee, R. López, M.-S. Choi, T. Jonckheere, and T. Martin, *Phys. Rev. B* **83**, 201304(R) (2011).

- <sup>21</sup> M. Filippone and C. Mora, Phys. Rev. Lett. **86**, 125311 (2012).
- <sup>22</sup> J. Wang, B. G. Wang, and H. Guo, Phys. Rev. B **75**, 155336 (2007).
- <sup>23</sup> Y. Ban, E. Y. Sherman, J. G. Muga, and M. Büttiker, Phys. Rev. A **82**, 062121 (2010).
- <sup>24</sup> M. Albert, C. Flindt, and M. Büttiker, Phys. Rev. Lett. **107**, 086805 (2011).
- <sup>25</sup> M. Albert, G. Haack, C. Flindt, and M. Büttiker, Phys. Rev. Lett. **108**, 186806 (2012).
- <sup>26</sup> K. H. Thomas and C. Flindt, Phys. Rev. B **87**, 121405(R) (2013).
- <sup>27</sup> Y. M. Blanter and M. Büttiker, Phys. Rep. **336**, 1 (2000).
- <sup>28</sup> A. Prêtre, H. Thomas, and M. Büttiker, Phys. Rev. B **54**, 8130 (1996).
- <sup>29</sup> M. Büttiker, Phys. Rev. B **45**, 3807 (1992); *ibid.* **46**, 12485 (1992).
- <sup>30</sup> Y. Levinson, Phys. Rev. B **61**, 4748 (2000).
- <sup>31</sup> H. Haug and A.-P. Jauho, *Quantum Kinetics in Transport and Optics of Semiconductors* (Springer-Verlag, Berlin, 1996).
- <sup>32</sup> B. G. Wang, J. Wang, and H. Guo, Phys. Rev. Lett. **82**, 398 (1999).
- <sup>33</sup> Z. S. Ma, J. Wang, and H. Guo, Phys. Rev. B **59**, 7575 (1999).
- <sup>34</sup> P. W. Brouwer and C. W. J. Beenakker, Phys. Rev. B **55**, 4695 (1997).
- <sup>35</sup> M. Büttiker, Phys. Rev. B **41**, 7906 (1990).
- <sup>36</sup> K. A. Matveev, Phys. Rev. B **51**, 1743 (1995).